Biochemistry

Article

pubs.acs.org/biochemistry

Remodeling of the Binding Site of Nucleoside Diphosphate Kinase Revealed by X-ray Structure and H/D Exchange

Alain Dautant,[†] Julien Henri,[§] Thomas E. Wales,[‡] Philippe Meyer,[§] John R. Engen,[‡] and Florian Georgescauld*[,§]

[†]Université de Bordeaux, CNRS, Institut de Biochimie et Génétique Cellulaires, UMR5095, 146 rue Léo Saignat, 33077 Bordeaux, France

[‡]Department of Chemistry and Chemical Biology, Northeastern University, Boston, Massachusetts 02115, United States

[§]Sorbonne Universités, UPMC Univ. Paris 06, CNRS, Laboratoire de Biologie Moléculaire et Cellulaire des Eucaryotes, UMR8226, Institut de Biologie Physico-Chimique, 13 rue Pierre et Marie Curie, 75005 Paris, France

Supporting Information

ABSTRACT: To be fully active and participate in the metabolism of phosphorylated nucleotides, most nucleoside diphosphate kinases (NDPKs) have to assemble into stable hexamers. Here we studied the role played by six intersubunit salt bridges R80−D93 in the stability of NDPK from the pathogen *Mycobacterium tuberculosis* (*Mt*). Mutating R80 into Ala or Asn abolished the salt bridges. Unexpectedly, compensatory stabilizing mechanisms appeared for R80A and R80N mutants and we studied them by biochemical and structural methods. The R80A mutant crystallized into space group *I*222 that is unusual for NDPK, and its hexameric structure revealed the occurrence at the trimer interface of a stabilizing hydrophobic patch around the mutation. Functionally relevant, a trimer of the R80A hexamer showed a remodeling of the binding site. In this conformation, the cleft of the active site is more open, and then active His117 is more accessible to substrates. H/D exchange mass spectrometry analysis of the wild type and the R80A and R80N mutants showed that the remodeled region of the protein is highly solvent accessible, indicating that equilibrium between open and closed conformations is possible. We propose that such equilibrium occurs *in vivo* and explains how bulky substrates access the catalytic His117.

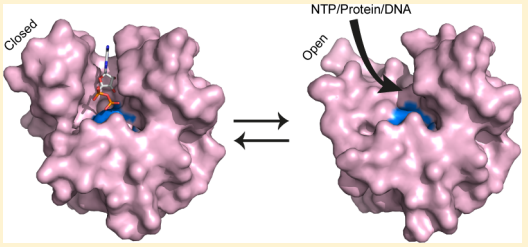

Nucleoside diphosphate kinases (NDPKs) are metabolic enzymes encoded by NME genes, also called NM23. They are present in all kingdoms of life and in certain viruses. NDPKs are responsible for the transfer of the γ-phosphate from nucleoside triphosphates (NTPs) to nucleoside diphosphates (NDPs), and in this way, they maintain the equilibrium between the pools of phosphorylated nucleosides (NTPs and NDPs).[1] The γ-phosphate transfer reaction takes place in two steps according to a ping-pong mechanism, with transient phosphorylation of the enzyme on a 100% conserved histidine residue.[2,3] NDPK recognizes with low specificity all tri- and diphosphate nucleosides.[4] As expected from their intracellular concentrations, it has been shown that the major phosphate donor in the cell is the ATP while the major acceptor is the GDP.[1] In mammals, by efficiently supplying with GTP the dynamin superfamily through direct interaction, researchers have recently shown that NDPK plays an important role in membrane remodeling and trafficking events.[5,6] Moreover, direct interaction between NDPK and different compounds or regulatory proteins from the cytoskeleton has been observed, indicating a clear role in nucleotide channeling and cell motility.[1,6]

Secondary enzymatic activities conserved from bacteria to humans have been established for NDPK. It can act as a protein histidine kinase,[7] bind to single-stranded DNA, and exhibit 3′−5′ exonuclease activity, playing a potential role in DNA repair.[8] Studies of *Drosophila*, zebrafish, and mice show a role of NDPK in early, larval, and embryo development.[9] In mammals, 10 different NDPK isoforms exist. Isoforms 1−7 were characterized and present at least one of the enzymatic activities, while the function of isoforms 8−10 is less understood.[1,8] Isoform 1, also known as NM23-A, is the most abundant one and was the first human metastasis suppressor to be reported.[10−12] The molecular mechanism by which NM23-A inhibits *in vivo* the metastasis from spreading is largely unknown and has been linked to the role of NDPK in cell motility. However, the metastasis suppression function is dependent on the capacity of NDPK to perform its enzymatic activities:[1] nucleoside diphosphate kinase,[13] histidine kinase,[7,14−16] and 3′−5′ exonuclease.[8,17,18]

To be functional, NDPK monomers have to autoassemble into hexameric or tetrameric complexes, sub-oligomeric species like monomers or dimers presenting at most 1−2% of the total activity.[19] Hexamers are formed in eukaryotes, archaea, some viruses, and Gram-positive bacteria,[20] while two different types

Received: December 26, 2018
Revised: February 5, 2019
Published: February 20, 2019

DOI: 10.1021/acs.biochem.8b01308
Biochemistry XXXX, XXX, XXX−XXX

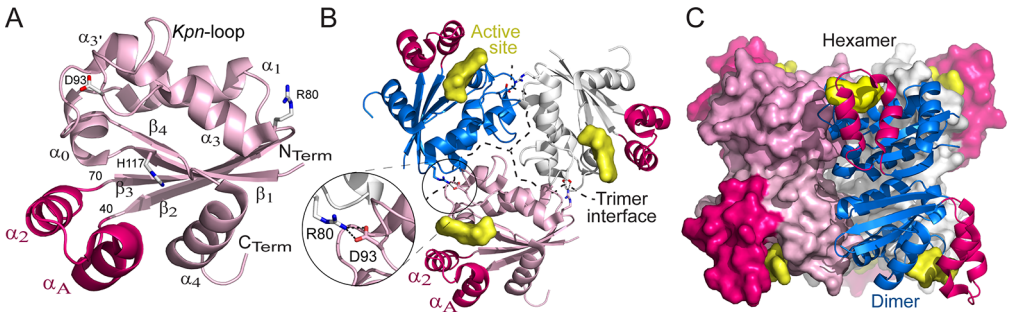

Figure 1. View along the 3-fold axis of (A) a monomer and (B) a trimer of wild-type *Mt*-NDPK (PDB entry 1k44).[24] The helix hairpin formed by helices α_A and α_2 that link the second strand to the third strand of the central β-sheet is colored magenta. The intersubunit salt bridges R80−D93 contribute to the high stability of *Mt*-NDPK. The trimer interface is drawn as a dashed line. ADPs bound in the active sites are drawn as yellow surfaces by homology with NDPK-A.[37] (C) Overall view of the hexamer. Two dimers are shown as pink and white surfaces, while the third is shown as a blue ribbon. The pink monomer shown in panels A and B is now at the bottom left of hexamer. This figure was drawn using PyMOL.[50]

of tetramers are present in Gram-negative bacteria.[21] In terms of the subunit composition of complexes, NDPK hexamers as well as tetramers are homo-oligomeric or hetero-oligomeric.[19] Interestingly, hetero-oligomers are formed *in vivo* as well as *in vitro*, from different cellular isoforms, after infection from a mix of host and pathogen monomers, a potential way to have more interactions with other proteins and hence more cellular functions.[19,22] All NDPK structures deposited at the Protein Data Bank (PDB) concern homo-oligomers. Figure 1A shows one monomer. The ferredoxin fold is conserved with two additional specific elements: the helix hairpin formed by helices α_A and α_2 linking strands β_1 and β_2 and the *Kpn* loop (named from the *Killer of prune* lethal mutation in *Drosophila*[23]) inserted between helices α_3 and $\alpha_{3'}$.[4,21] All structures show that monomers are in the same conformation inside the hexamers or tetramers, in agreement with the idea that active sites are identical and independent.

Complete genome sequencing of *Mycobacterium tuberculosis* (*Mt*), the causative agent of tuberculosis, showed that it contains only one gene encoding NDPK (UniProtKB entry A5U5E1), and its crystal structure showed it forms hexamers [PDB entry 1k44 (Figure 1)].[24] In patients infected with tuberculosis, the bacterium is phagocytosed by macrophages but escapes degradation by preventing the fusion of the phagosome with the lysosome.[25] The escape mechanism responsible for enhanced intracellular survival within macrophages is not fully understood but requires several thermostable proteins,[26] including NDPK.[25,27] In this context, we previously studied the stabilizing mechanisms allowing *Mt*-NDPK to present a 15−20 °C higher T_m compared to those of NDPKs from other species.[20] We showed that this unusually high stability is partially based on the presence of six intersubunit ionic bridges R80−D93 (Figure 1B). When the bridges were abolished by the D93N point mutation, the mutant was still hexameric and enzymatically active, but its T_m dropped by 28 °C.[20] Equilibrium analysis of the wild type (WT) and D93N mutant by hydrogen/deuterium exchange mass spectrometry (HDX-MS) allowed us to show that the R80−D93 bridge was not only important with respect to hexamer stability but also influenced its conformational dynamics.[28]

We have continued our research to understand the role of ionic bonds in *Mt*-NDPK stability and conformational dynamics by mutating R80, the other amino acid involved in ionic bridge formation (Figure 1B). Mutants R80A and R80N (R80A/N) were produced, and their properties studied by enzymology, fluorescence, circular dichroism (CD), and size-exclusion chromatography (SEC). The structure of mutant R80A that crystallized into an unusual space group for NDPKs was determined. We noticed important conformational remodeling that has not been stated so far. It mainly concerned peripheral helices α_A and α_2 that are involved in nucleotide binding and in it being locked inside the active site. In the current structure, the catalytic site is remodeled and becomes accessible for substrates larger than a nucleotide. To show that such a conformational change exists in solution, we performed at equilibrium HDX-MS measurements for WT, R80A, and R80N in the presence and absence of nucleotides. The HDX data that illuminated *Mt*-NDPK dynamics in solution were in perfect agreement with the structural remodeling observed in the crystal structure. We propose that the highlighted conformational change explains how bulky substrates access the catalytic His117.

MATERIALS AND METHODS

Reagents. Chemicals of the highest purity grade were bought from Sigma. Solutions of urea were freshly prepared for each experiment.

Mutagenesis and Protein Purification. The R80A gene mutation was introduced using a Transformer site-directed mutagenesis kit (Clontech), and the mutation was confirmed by nucleotide sequencing. The individual expression of WT, R80A, R80N, and D93N *Mt*-NDPK recombinant proteins was realized using a pET24 vector (Novagen) in the BL21-derived host strain BL21-CodonPlusH(DE3)-RIL (Stratagene). The 2YT culture medium contained 16 g/L bacto tryptone, 10 g/L bacto yeast extract, and 5 g/L sodium chloride, in the presence of 80 mg/mL kanamycin. The expression was induced with 1 mM isopropyl β-D-1-thiogalactopyranoside for 6 h at 37 °C, once the optical density reached 0.5−0.7 unit. As previously described, the purification steps were carried out at 4 °C.[20,28] After being harvested, the *Escherichia coli* cells were sonicated and centrifuged to recover the soluble fraction containing *Mt*-NDPKs. The DNase-treated bacterial extract was loaded onto a Q-Sepharose column equilibrated in 100 mM Tris-HCl (pH 7.4). The enzyme was eluted at 0.5−0.6 M NaCl, in a linear gradient from 0 to 0.8 M NaCl in the same buffer. Active fractions were precipitated with 80% saturated ammonium sulfate and further purified by salting-out chromatography on a Sepharose 6B column equilibrated with 80% ammonium sulfate and 100 mM Tris-HCl (pH 7.4). The protein was eluted by a linear gradient from 80 to 20% ammonium sulfate

DOI: 10.1021/acs.biochem.8b01308
Biochemistry XXXX, XXX, XXX−XXX

in the same buffer. The active fractions were pooled, dialyzed against 100 mM Tris-HCl (pH 7.4), and further purified on a Source 15Q column, under the conditions described for Q-Sepharose chromatography. The enzymes were precipitated by dialysis against a saturated solution of ammonium sulfate, recovered by centrifugation, and further purified by SEC on a Sephacryl S-200 column equilibrated with 0.2 M sodium phosphate buffer (pH 7.0). This step allowed the sample to be cleaned up, by eliminating aggregated and dissociated protein. The enzymes were essentially pure as ascertained by polyacrylamide gel electrophoresis in the presence of sodium dodecyl sulfate. The concentrations of WT and mutant *Mt*-NDPKs were determined from the optical density at 280 nm using an extinction coefficient of 0.48 for 1 mg/mL, which was calculated from the amino acid composition. The molecular weight of proteins was checked by mass spectrometry.

Size-exclusion chromatograms were recorded on a Superose 12, 10/300 GL column equilibrated with 20 mM Tris-HCl (pH 7.0) and 100 mM NaCl to ensure that all proteins were hexameric. The following molecular markers were used: cytochrome *c*, 12.4 kDa; myoglobin, 17 kDa; carbonic anhydrase, 29 kDa; ovalbumin, 44 kDa; bovine serum albumin (BSA), 68 kDa; aldolase, 158 kDa; β-amylase, 200 kDa (GE Healthcare Life Sciences).

Thermal Denaturation and Chemical Unfolding Experiments. Thermal denaturation experiments were performed by incubating 10 μg/mL NDPK in a water bath and increasing the temperature at a rate of 1 °C/min. At different time points (corresponding to different temperatures), aliquots were taken and the enzyme activity was measured according to the NDPK enzymatic assay.

The chemical unfolding experiments were performed as previously described.[20,28] A 10 μg/mL final concentration of native or unfolded *Mt*-NDPK was incubated for 16 h in 0−8 M urea or 0−5 M GuHCl and 20 mM phosphate buffer (pH 7.0) at 25 °C. Fluorescence intensities of the single tryptophan residue, Trp132, were measured at 335 nm with excitation at 295 nm.

NDPK Enzymatic Assay. The enzymatic activity of NDPK was measured using a coupled assay that involves the three independent reactions shown below.[20] Enzymes performing the catalysis of each reaction are indicated in parentheses. NDPK catalyzed the transfer of the γ-phosphate from ATP to 8-bromoinosine 5′-diphosphate (8-BrIDP). The reaction took place in 0.8 mL of an enzyme mix containing 1 mM ATP, 0.2 mM 8-BrIDP, 1 mM phosphoenolpyruvate (PEP), 0.1 mM NADH, 20 mM Tris-HCl (pH 7.5), 5 mM $MgCl_2$, 100 mM KCl, 1 mg/mL BSA, 2 units/mL pyruvate kinase, and lactate dehydrogenase. The disappearance of NADH was measured at 340 nm and 25 °C, using a PerkinElmer spectrophotometer.

$$\text{ATP} + \text{8-BrIDP} \rightarrow \text{ADP} + \text{8BrITP (NDPK)}$$

$$\text{ADP} + \text{PEP} \rightarrow \text{ATP} + \text{pyruvate (pyruvate kinase)}$$

$$\text{pyruvate} + \text{NADH} \rightarrow \text{lactate} + \text{NAD}^+ \text{ (lactate dehydrogenase)}$$

Crystallization and X-ray Diffraction Data Collection. Recombinant *Mt*-NDPK-R80A was purified by Superdex 200 SEC in a buffer consisting of 100 mM NaCl and 20 mM Tris-HCl (pH 7.9). Collected peak fractions were pooled and concentrated to 12.1 mg/mL by ultrafiltration. Sparse-matrix screening of candidate crystallization conditions was set up on TTP Labtech IQ plates with mixes of 50 nL of protein and 50 nL of commercial precipitant solutions (Qiagen) and incubated at 20 °C. Monocrystalline 100 μm × 50 μm platelets of R80A *Mt*-NDPK grown for 5 weeks under condition JCSG IV 58 [0.8 M ammonium sulfate and 0.1 M HEPES-NaOH (pH 7.0)] were cryo-protected by addition of 25% glycerol and flash-frozen in liquid nitrogen. Two thousand images of a 0.1° rotation increment each were collected on the ID30A-3 MASSIF microfocus beamline at the European Synchrotron Radiation Facility (Grenoble, France) at 12.81 keV. Diffraction data were recorded on an Eiger X 4M detector. The data were indexed and integrated with IMOSFLM[29] and SCALA[30] in orthorhombic space group *I*222 with the following unit cell parameters: a = 113.1 Å, b = 121.7 Å, and c = 150.71 Å. The data set was complete to >99% at a resolution of 2.2 Å. The structure was determined by a molecular replacement method with MOLREP using the highest-resolution available *Mt*-NDPK structure (PDB entry 4ane) as a search model.[31] The unit cell contained six molecules in the asymmetric unit, resulting in a solvent content of 59% [Matthews coefficient (V_m) of 2.99 Å^3 Da^{-1}].

HDX-MS. Stock solutions of 4.0 μM native *Mt*-NDPKs (WT and R80A/N) were prepared in 20 mM Tris-HCl (pH 7.0), 100 mM NaCl, and H_2O. Deuterium exchange was initiated by 20-fold dilution of the *Mt*-NDPK stock solution into 100 mM NaCl, 20 mM Tris-HCl (pD 7.0), and 99.9% D_2O at 10 °C. At different incubation times, a 100 μL aliquot was removed from the exchange reaction mixture (from 10 s to 120 min) and labeling was quenched at pH 2.5 by adding 10 μL of a solution of 1% formic acid and 5 M GuHCl at 0 °C; 100 μL of each acid-quenched sample was immediately injected into an HDX Waters nanoACQUITY ultraperformance liquid chromatography (UPLC) instrument.[32] The sample passed through a Poroszyme-immobilized pepsin cartridge (Applied Biosystems) accommodated within the HDX manager at a flow rate of 100 μL min^{-1} and 15 °C. Peptic peptides eluting from the pepsin column were trapped and desalted for 3 min at a rate of 100 μL min^{-1}. Peptides were separated in 6 min with a 5 to 35% acetonitrile/water gradient in 0.1% formic acid, at a rate of 100 μL min^{-1} with a 1.0 mm × 50.0 mm ACQUITY UPLC C18 HSS T3 column (Waters) containing 1.8 μm particles (back pressure of 13000 psi). All chromatographic elements were held at 0 °C for the entire time of the measurements. The calculated average amount of back exchange was 31% on the basis of analysis of fully deuterated peptides of NDPK in GuDCl. Because all comparison experiments were performed under identical experimental conditions, there was no correction for back exchange.[33] The error in the determination of the deuterium levels was ±0.20 Da in this experimental setup, consistent with previously obtained values.[34,35] Mass spectra were recorded in HDMS^E mode using a Waters Synapt G2 Si instrument with a standard ESI source (Waters Corp., Milford, MA) over an m/z range of 50−2000. Mass accuracy was ensured by calibration with the Glu-fibrinogen peptide and was <10 ppm throughout all experiments. Identification of the peptic fragments was accomplished with at least four replicate HDMS^E analyses using PLGS 3.0 (Waters Corp.). Deuteration experiments were performed between two and four times. Mass spectra were processed using DynamX 3.0 (Waters). Automated selection of the isotope distribution was verified manually for all peptides and all charge states. The resulting relative deuterium levels

DOI: 10.1021/acs.biochem.8b01308
Biochemistry XXXX, XXX, XXX−XXX

Table 1

Mt-NDPK	T_m (°C)	specific activity (units/mg)	PDB entry	resolution (Å)	solvent content (%)	space group	ref
WT	76.1	550	1k44	2.6	56	$P2_12_12_1$	24, 28
D93N	48.4	230	4anc	2.8	68	$P4_332$	20, 28
			4and	2.8	66	$P2_13$	
R80N	69.3	320	4ane	1.9	47	$I2$	51
R80A	69.0	350	6qa2	2.2	59	$I222$	this work

were plotted versus the exchange-in time with respect to the described experimental conditions.

RESULTS AND DISCUSSION

Biochemical and Enzyme Properties of R80A/N *Mt*-NDPK. We previously studied the biochemical and enzyme properties of WT and D93N *Mt*-NDPK.[20] Now, recombinant R80A and R80N *Mt*-NDPK were overexpressed in *E. coli* and purified without a tag. The mass of monomers was verified by mass spectrometry, and using SEC, we established that all proteins formed hexamers (Figure S1). Ultraviolet (UV), tryptophan fluorescence, and CD spectra were identical between WT and R80A/N. The enzyme specific activities of mutants were 350 and 320 units/mg, respectively (Table 1), close to that of the WT protein. Taken together, these results suggested that mutations did not significantly affect the overall three-dimensional protein structure and NDPK stability was studied next.

Mutation of Amino Acids Involved in the Intersubunit Salt Bridges (R80 vs D93) Has a Different Effect on *Mt*-NDPK Hexamer Stability. WT *Mt*-NDPK exhibited a thermal stability 15−20 °C higher than that of NDPK from other organisms.[24] We previously showed that this stability is based on six intersubunit salt bridges R80−D93 (Figure 1B) and their abolishment through mutation D93N, inducing a loss of stability of 28 °C. Now, we abolished the bridges through mutations R80A and R80N and followed the thermal stability by enzyme activity. The T_m for the WT was 76 °C, in agreement with previously published results.[20] R80A and R80N both exhibited T_m values of 71 °C, indicating a loss of stability of only 8 °C. Such a difference in the thermal stability of mutants D93 and R80 when both residues are involved in the intersubunit salt bridges was puzzling.

To better understand the role of the salt bridge R80−D93, we next measured the stability of the WT and mutants in the presence of two different denaturant reagents: urea, a non-ionic reagent, and guanidinium hydrochloride salt (GuHCl). Proteins were incubated for 16 h at different denaturant concentrations, and unfolding curves were recorded following the Trp fluorescence as well as the enzymatic activity.

Following the intensity in Trp fluorescence reflects changes in the tertiary structure because *Mt*-NDPK is a unidomain protein and contains a unique Trp132 that is buried far from subunit interfaces. During unfolding, WT and R80A/N exhibit a unique transition from the folded state (at a low urea concentration) to the unfolded state (at a higher urea concentration) (Figure 2A). We noticed that denaturation of R80A/N occurred at a urea concentration ($c_{1/2}$ of 4.0 M) lower than that of the WT ($c_{1/2}$ of 5.5 M). As already published[20] and in agreement with the thermal denaturation, D93N was the less stable ($c_{1/2}$ of 2.5 M). A similar result for hexamer stability was obtained in the presence of GuHCl (Figure S2A).

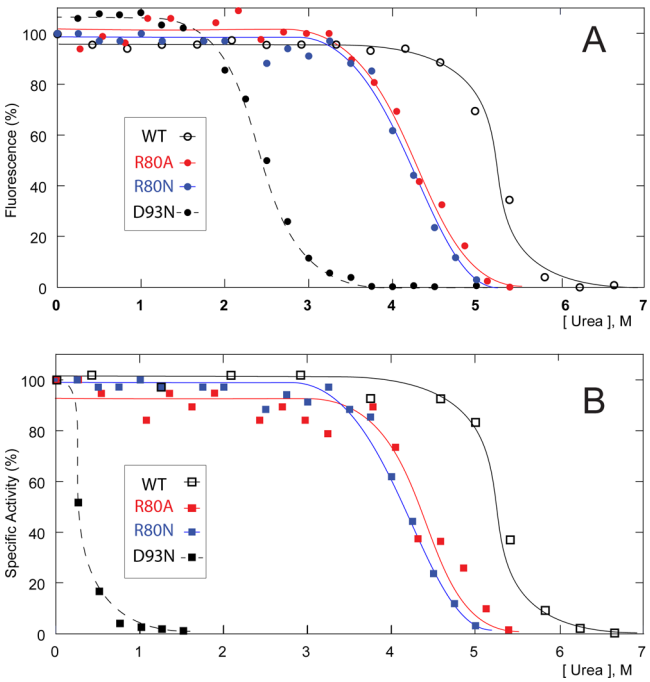

Figure 2. Unfolding pathway of WT, R80A, R80N, and D93N *Mt*-NDPK monitored by (A) intrinsic fluorescence and (B) residual enzymatic activity. Each sample was preincubated for 16 h in the presence of 0−7 M urea.

The enzymatic activity is strictly dependent on the presence of quaternary structure, meaning on correct assembled hexamers.[19] Studying properties of natural mutants of NDPK from multiple species, different groups showed using SEC that such mutants can accumulate as stable monomers or dimers and present at most 1−2% of the hexamer activity.[23,36−38,45] Figure 2B shows that the WT is inactivated at 5.3 M urea while R80A and R80N are inactivated at 4.2 M urea, indicating that hexamers of WT are more stable than those of the mutants. Because the loss of activity and Trp fluorescence changes appear at similar urea concentrations for each NDPK, these results indicate that hexamers disassemble and unfold concomitantly, without accumulation of dissociated species. D93N hexamers exhibit a different behavior. As published, activity is lost at 0.3 M urea while a decrease in fluorescence appears at 2.5 M urea, indicating that hexamers disassemble before unfolding.[20]

The stability of WT, R80A/N, and D93N hexamers was measured by the same procedure in the presence of GuHCl (Figure S2B). The WT was more stable than the three mutants. R80A and R80N exhibited similar stability but were more stable than D93N, a behavior similar to that determined in the presence of urea. Taken together, the results from both thermal stability and chemical stability show that mutating R80 or D93 to abrogate R80−D93N salt bridges has a different

DOI: 10.1021/acs.biochem.8b01308
Biochemistry XXXX, XXX, XXX−XXX

effect on NDPK stability. This suggested that compensatory effects exist for R80A/N but not for D93.

Structural Remodeling of Three Subunits inside the NDPK Hexamer Is Revealed by the Structure of the R80A Mutant. To understand the different effect of mutations R80A/N and D93N on hexamer stability, we next focused on the *Mt*-NDPK structure analysis. Structures were available for WT, R80N, and D93N (Table 1), and we determined here the structure of the R80A mutant at 2.2 Å resolution. Table 2 summarizes the X-ray data processing and refinement statistics. The crystals belong to the *I*222 space group with a single hexamer in the asymmetric unit. A one-dimensional infinite solvent channel with a cross section of 60 Å × 30 Å along the *a* axis results in a high solvent content of 59% (Table 1 and Figure S3A). Only two other NDPK structures in the PDB (entries 4w98 and 4wbf) belong to this space group but in a different crystal packing. They both concern the NDPK from the bacterium *Acinetobacter baumannii*, a potential dimer from SEC experiments.[36]

Table 2. Crystallographic Statistics for PDB Entry 6QA2[a]

Data Collection	
wavelength (Å)	0.961
space group	*I*222
unit cell dimensions *a*, *b*, *c* (Å)	113.1, 121.7, 150.71
resolution range (Å)	34.07−2.20 (2.32−2.20)
no. of unique reflections	52205 (7546)
R_{merge}[b] on *I* (%)	14.2 (78.7)
R_{meas}[c] on *I* (%)	15.2 (84.3)
R_{pim}[d] on *I* (%)	5.4 (29.9)
$I/\sigma(I)$	10.4 (3.1)
Wilson *B* (Å^2)	25.65
completeness (%)	98.6 (99.1)
multiplicity	7.4 (7.6)
Model and Refinement	
no. of reflections (total, test)	52182 (2475), 2578 (127)
R_{cryst}/R_{free}[e] (%)	18.1/20.9
no. of protein residues/atoms	768/5717
no. of waters/sulfates/Tris atoms	467/60/22
B values[f] (Å^2)	
average isotropic *B* (overall)	40.3
protein overall	39.8
all main/side chains	37.8/42.1
water/sulfate/Tris	39.1/94.3/73.3
rmsd[g]	
bond lengths (Å)	0.002
bond angles (deg)	0.49
Ramachandran analysis (%)	
favored regions	97.77
allowed regions	2.33
outliers	0.0

[a]Values in parentheses are for the highest-resolution shell. [b]$R_{merge} = \sum_{hkl}\sum_i|I_i(hkl) - \langle I(hkl)\rangle|/\sum_{hkl}\sum_i I_i(hkl)$. [c]$R_{meas} = \sum_{hkl}[N/(N-1)]^{1/2}\sum_i|I_i(hkl) - \langle I(hkl)\rangle|/\sum_{hkl}\sum_i I_i(hkl)$. [d]$R_{pim}$ (precision-indicating R_{merge}) $= \sum_{hkl}[1/(N-1)]^{1/2}\sum_i|I_i(hkl) - \langle I(hkl)\rangle|/\sum_{hkl}\sum_i I_i(hkl)$, where *N* is the multiplicity of reflection *hkl* and $I_i(hkl)$ and $I(hkl)$ are the intensity of the *i*th measurement and the average intensity of reflection *hkl*, respectively. [e]R_{cryst} and $R_{free} = \sum||F_{obs}| - |F_{calc}||/\sum|F_{obs}|$ for reflections in the working and test sets, respectively, where F_{obs} and F_{calc} are the observed and calculated structure factor amplitudes, respectively. R_{free} is the same as R_{cryst} but for 5% of the total reflections chosen at random and omitted from structural refinement. [f]The average isotropic *B* includes TLS and residual *B* components. [g]Root-mean-square deviation.

On the 3-fold axis of the molecule, two Tris molecules are bound by Arg25, Arg28, and Asp106 side chains, and on the outer surface, sulfate ions are bound by each Arg86. A sulfate ion has also been modeled into each binding site as a ligand of His117, Arg104, and Arg86 (Figure S3B). Residual densities around this sulfate ion suggest the alternative presence of water, Tris, or HEPES molecules, but attempts to incorporate them into the model were not fully successful. Around mutation R80A, the trimer interface becomes highly hydrophobic, with a patch containing A80, A83, and A84 on one face and V95 and L109 on the other face (Figure S3C).

R80A adopted a conserved ferredoxin fold of ∼90 amino acids, formed by four antiparallel β-strands and two connecting α-helices (α_1 and α_3) that cover one face of the β-sheet (Figure 3A). Residues 92−112 form the *Kpn* loop that contains a turn of a 3_{10} helix, a turn of a polyproline II left-handed helix, and a turn of a standard α-helix. The *Kpn* loop is followed by strand β_4 that contains the active site His117. The monomers, trimers, and hexamer are similar to the WT ones with root-mean-square deviations (rmsd's) of 0.24−0.36, 0.45, and 0.61 Å for 100, 300, and 600 C_α atoms excluding amino acids 41−70, respectively. In trimer I (chains A, C, and E), the other face of the β-sheet was covered by the helix hairpin formed by helices α_A (amino acids 43−53) and α_2 (amino acids 58−65) like in the WT structure (magenta in Figure 1A for WT and green, cyan, and orange in Figure 3A,B for R80A) (rmsd of 0.29 Å for 30 C_α atoms of amino acids 41−70), whereas in trimer II (chains B, D, and F), the backbone from Thr40 to Gly69 was fully remodeled (Figure 3C,D) (rmsd of 4.31 Å for 30 C_α atoms of trimer I and WT). This remodeling consisted of (i) the complete unfolding of α_A, (ii) the conformational change of helix α_2 in successive β-turns of types I and II, and (iii) the increase in the length of strands β_2 and β_3 with formation of weak hydrogen bonds between the main chain carbonyl oxygen and amide nitrogen of residues 41 and 69 (Figure 3C,D). Helices α_A and α_2 contained one active site amino acid each, Tyr50 and Phe58, respectively. Phe58 (C_α) was shifted by 3.5 Å, and Tyr50 (C_α) by >15 Å. Phe65, which was far from the essential His117 (11.5 Å between C_β atoms) in the closed conformation, moves to stack on the His117 imidazole ring (3.5 Å) on the open one.

NDPK structures containing a bound nucleotide show that it is sandwiched between the helix hairpin and the *Kpn* loop[37] (Figure 1B,C). Amino acids involved in the nucleotide binding site are highly conserved, forming a well-defined cleft that is perfectly filled by one single phosphorylated nucleoside at a time. Because of this restricted space, one long-standing question concerning NDPK histidine kinase activity has been how bulky protein substrates can access the active site, up to the deep buried essential His117. In such an open conformation, the substrate binding loop is partially folded and the active site is easily accessible (Figure 3B,D).

In the R80A crystal, the hairpin helices of trimer I (brown surface) are fully buried and involved in crystal contacts, like in WT. In trimer II, they are fully exposed to the solvent channel without crystal contacts (magenta surface) (Figure S3D). According to the crystal packing, the remodeled regions are not influenced by crystal contacts, suggesting that in solution such conformations are possible. In trypanosomatid parasites, *Leishmania*, and *Giardia lamblia* NDPKs, these helices are not

DOI: 10.1021/acs.biochem.8b01308
Biochemistry XXXX, XXX, XXX−XXX

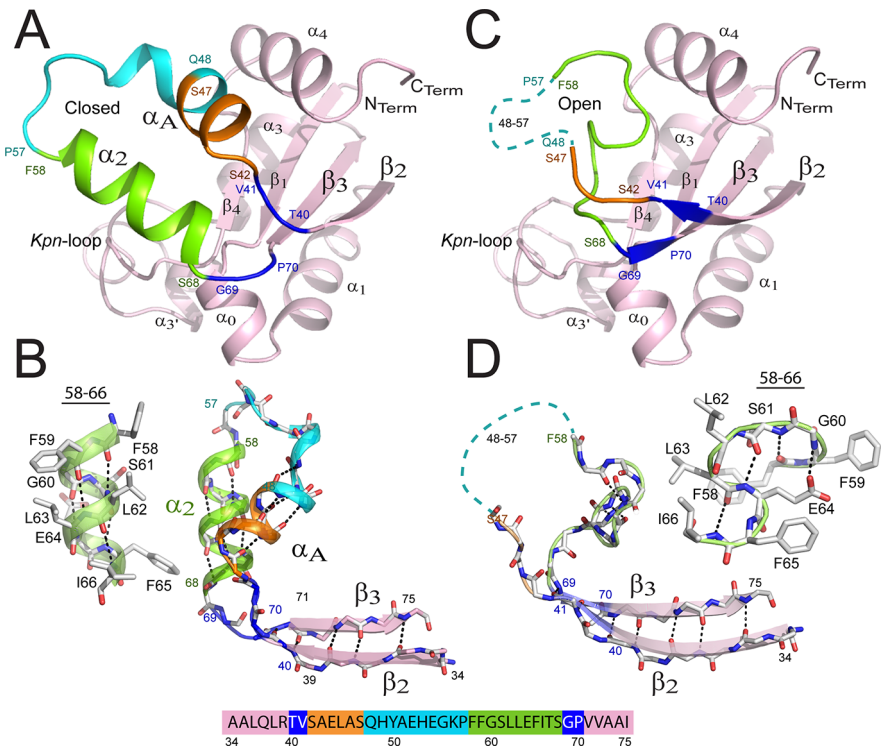

Figure 3. (A) View of a monomer of chains A, C, and E and (C) view of a monomer of chains B, D, and F. The $\beta_2\alpha_A\alpha_2\beta_3$ region is remodeled in the latter monomers, and details are provided in panels B and D, respectively. Residues 40 and 41, 42−47, 48−57, 58−68, and 69 and 70 are colored blue, orange, cyan, green, and blue, respectively. The region covering residues 48−57 is not visible in the X-ray structure for monomers B, D, and F and is shown as a cyan dashed line in panels C and D. The α_2 helix (B) and the successive β-turn structures (D) are shown as cartoons and ball-and-stick structures.

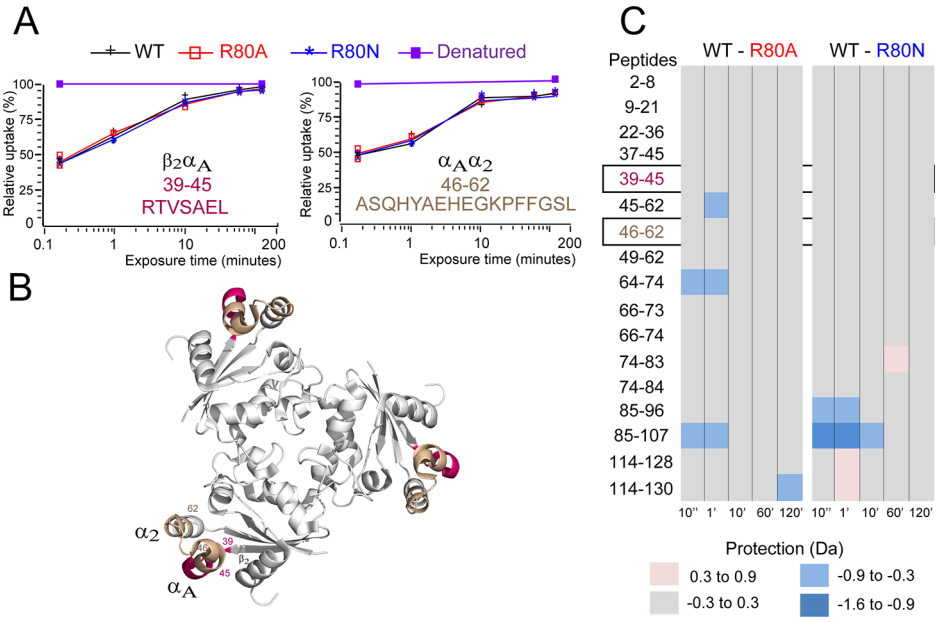

Figure 4. (A) Representative deuterium incorporation curves, including error bars, for peptides covering residues 39−45 and 46−62. The purple vertical line shows the maximal deuteration obtained experimentally for these peptides in the denatured state. (B) Top view showing the NDPK trimer. Residues covering amino acids 39−45 and 46−62 are colored magenta and brown, respectively. (C) Comparisons of relative deuterium exchange in WT vs R80A (left) and WT vs R80N (right). All relative differences are shown in daltons and color-coded according to the scale at the bottom. The left side shows the residue numbers of each peptide fragment, arranged in order from the N- to C-terminus (top to bottom, respectively). The deuterium incorporation graphs used to create this figure are shown in Figure S4B. Within both panels, the differences in uptake at various times, from 10 s to 120 min, are shown and indicated at the bottom of each panel.

visible in the electron densities and were likely fully disordered.[38,39]

HDX-MS Revealed Full Solvent Accessibility Only for the *Mt*-NDPK Region That Can Be Remodeled. The next

DOI: 10.1021/acs.biochem.8b01308
Biochemistry XXXX, XXX, XXX−XXX

question we answer is whether *Mt*-NDPK conformational changes observed by crystallography can be monitored in solution. HDX-MS is a method that has been applied to follow conformational changes and dynamics for many proteins,[33,40−42] including serine, threonine, and tyrosine kinases.[43,44] However, so far, only one study by from our group used HDX-MS to study NDPK, which belongs to the histidine kinase family.[28] We showed in this study that during folding dimers of D93N and WT *Mt*-NDPK are stably formed. They are nativelike except for the minor subdomain (Kpn/α_0), part of the active site, which is unfolded in the dimer and becomes structured only upon hexamerization. HDX-MS relies on the natural property that proteins rapidly exchange their backbone amide hydrogen atoms that are not involved in stable H-bonds and are accessible to a solvent water catalyst. Exposing a protein of interest to a solvent containing D_2O induces rapid replacement of the labile accessible backbone with deuterium (D). To spatially reveal where the exchange has happened, the incorporation of deuterium is measured by MS analysis after protein digestion and interpreted in light of the structure, if it is available.[41]

The *Mt*-NDPK conformational changes revealed by crystallography concerned the region covering amino acids 40−70. We hypothesized that if in solution the NDPK shifts from one conformation to the other, maximal deuteration should be observed for this region. Here, we applied continuous labeling HDX-MS to native hexamers of WT, R80A, and R80N *Mt*-NDPK (see SEC in Figure S1). Samples were incubated at 10 °C from 10 s to 120 min in a buffer mimicking their physiological environment and containing a D_2O final concentration of 95%. At different time points of deuteration, aliquots were taken, acid quenched, pepsin digested, separated by LC, and immediately introduced into a mass spectrometer for mass analysis.

There were 37 peptic peptides identified for the three proteins, and 15 of these peptides that were common to the three proteins were routinely analyzed by HDX (see the peptide map in Figure S4A). The region of amino acids 75−83 containing the site of mutation was covered for the WT and mutant proteins by three different peptides. The final sequence coverage was 91.2% for WT and R80N and 90.4% for R80A. The last six C-terminal residues covering amino acids 131−136 were not detected in these experiments with IMS. Previously, this region of the protein was maximally deuterated within 10 s.[28]

EX2 exchange was noticed with no exception for all peptides of WT and R80A/N (Figure S4B), in agreement with our previous study of WT and D93N.[28] Deuterium incorporation plots were almost identical for the common peptides of the three proteins, and an increased deuteration level with time was observed for all analyzed peptides (Figure S4B for common peptides and peptides covering the mutation). When compared to values of maximal deuteration obtained from controls of fully denatured and deuterated NDPK in GuDCl, the region covering amino acids 39−62 was the only one for all three proteins to be flexible enough during the labeling experiment to reach maximal deuteration. Figure 4A illustrates the behavior of peptides 39−45 and 46−62 covering this region. Similar behavior was noticed for three redundant peptides covering this region (see peptides 37−45, 45−62, and 49−62 in Figure S4B). Because the maximal deuteration level appeared with a similar trend for these five peptides, this indicates that the region formed a subdomain showing high cooperativity. Importantly, this region is the one containing helices α_A and α_2, which in the R80A crystal structure presented the conformational change (Figure 4B). Therefore, HDX-MS and crystallography give evidence of the high flexibility of this region of the protein that is essential for the full activity of NDPK. The other peptides of the three proteins showed for time points of <10 min modest deuteration, which was <50% of maximal deuteration (Figure S4B). The weakest exchange was noticed for peptides covering amino acids 2−36, which incorporated during 2 h <4 Da over 31 Da exchanged in the denatured peptides (<13% total deuteration). This indicates that a very stable core with modest dynamics exists in this area of the hexamer (amino acids 2−36). Interestingly, from an evolutionary point of view, this NDPK region is one of the most conserved.

We analyzed next the effect of the mutations R80A and R80N on the dynamics of the hexamer. The chicklet shown in Figure 4C indicates peptide by peptide the difference for all time points between WT and R80A and between WT and R80N. Interestingly, both mutants had dynamics very similar to those of the WT, except for the region covering amino acids 85−107 that was more dynamic in both mutants (Figure S4C). This region corresponds to the *Kpn* loop, a specific structure in NDPK known to be involved in hexamer stability and hexamer assembly.[28] While a plateau of 7 Da incorporation was reached for this region after deuteration for 2 h for R80A/N, the same plateau was reached within 10 s for D93N.[28] This indicates that mutation D93N that is thermodynamically more destabilizing than mutations R80A and R80N induced a higher flexibility not only around the mutation itself but also for the subdomain that contains it. Altogether, these results showed a strong correlation between protein stability and protein dynamics for the *Mt*-NDPK.

NDPK hexamers are fully phosphorylated by NTPs on catalytic histidine.[2,3] We phosphorylated WT and R80A/N *Mt*-NDPK over 3 min by addition of ATP, followed by incubation in a D_2O solution as previously described. Peptide deuteration plots for the phosphorylated versus nonphosphorylated proteins were identical, indicating that no conformational changes were induced by protein phosphorylation (Figure S4C). Similarly, no conformational changes were detected by continuous labeling HDX-MS after binding of AMP-PNP, a nonhydrolyzable analogue of ATP, to any of the three proteins (data not shown).

CONCLUSIONS

In most organisms, a majority of proteins are oligomers, their percentages increasing from bacteria to eukaryotes. Importantly, these assemblies have to be stable enough to perform their functions over different periods of time, which can stretch from minutes to years. Here we studied the role of intersubunit salt bridges R80−D93 in the stability of *Mt*-NDPK hexamers. Surprisingly, mutation of R80 or D93, each of which broke the salt bridge, did not have the same influence on hexamer stability, and compensatory mechanisms appeared. The D93N mutant was strongly destabilized, showing critical role of amino acids that belong to the *Kpn* loop (amino acids 92−112), while R80A and R80N were almost as stable as WT. The higher stability of the R80N mutant can be explained by the hydrogen bonds between the side chain of Asn80 and (i) the main chain carbonyl of Leu109 from the neighboring subunit and (ii) moreover the Asp93 carboxyl group via a water molecule. In the R80A mutant, these two bonds were absent

DOI: 10.1021/acs.biochem.8b01308
Biochemistry XXXX, XXX, XXX−XXX

and the hydrophobic patch around the mutation compensated for the loss of the salt bridge (Figure S3C).

During evolution, stabilization of NDPK complexes was performed by mechanisms that were different from organism to organism. In the NDPK from *Dictyostelium discoideum*, the quaternary structure counteracts the tendency of monomers to form molten globule structures.[45] For the hyperthermophile bacteria *Aquifex aeolicus*, the stabilization of NDPK is realized through formation of intersubunit disulfide bridges,[46] while for the hyperthermophile archaea *Pyrobaculum aerophilum*, it is performed with the help of two additional specific domains.[47] Dimers of NDPK present a more modest stability compared to those of hexamers and tetramers.[48,49] In this context, our study of *Mt*-NDPK showed a new stabilizing mechanism based on the presence of nonconserved intersubunit salt bridges R80−D93. Additionally, using HDX-MS methodology, we also showed a strong correlation for *Mt*-NDPK between protein stability and protein flexibility: the highest stability has the lowest flexibility.

According to its major enzymatic function in nucleotide homeostasis, the correct biochemical name of NDPK should be NTP/NDP transphosphorylase. Besides this function, NDPK has secondary functions as a protein histidine kinase[7,14−16] and a 3′−5′ exonuclease.[8,17,18] For the histidine kinase activity, at least three defined substrates have so far been described: the β subunit of heterotrimeric G proteins, the intermediate conductance K^+ channel K(Ca)3.1, and the Ca^{2+}-conducting TRP channel family member, TRPV5. With regard to the mechanism for the histidine kinase activity, a direct transfer of phosphate from the phosphorylated histidine (His117) in the active site of NDPK and the histidine in the substrate protein has been proposed.[7] It is reasonable to assume that an opening of the active cleft must occur from the closed conformation, to allow the entry and the interaction of the target polypeptide with the NDPK catalytic His117. In all available structures of NDPK, the $\alpha_A-\alpha_2$ hairpin has atomic displacement parameters (*B* factors) higher than those of the rest of the protein. If the hairpin is involved in interhexamer contacts within the crystal, its electron density is strong. In some extreme cases, the density partially or totally disappears, the hairpin being fully unfolded.[38,39]

One NDPK presenting histidine kinase activity is the mammalian isoform Nm23-H2. Several structures of Nm23-H2 are available: one apo form, which is closed (PDB entry 1nue), one containing GDP, which is slightly more open (PDB entry 3bbf), and one with the most open cleft containing a dinucleotide (PDB entry 3bbb). The comparison of these structures of Nm23-H2 has highlighted the progressive opening of the $\alpha_A-\alpha_2$ hairpin without unfolding, and a model of interaction between Nm23-H2 and the c-myc gene has been proposed.[52] For the R80A mutant of *Mt*-NDPK, the mutation induced an original crystal packing with a large solvent channel where the $\alpha_A-\alpha_2$ hairpin can unfold and refold in a new conformation with different secondary structures (Figure 3). The histidine kinase activity of *Mt*-NDPK has never been observed, but a secondary function of 3′−5′ exonuclease has been demonstrated.[53,54] We overlapped the remodeled structure of the R80A mutant with three other NDPK structures: the apo WT from *M. tuberculosis*, the apo human WT isoform Nm23-H2, and the human WT isoform Nm23-H2 in complex with a dinucleotide (Figure S5A). Differences between these structures can be noticed, and they exemplify the dynamic behavior and the plasticity of the hairpin. We stress that the R80A structure presents the most open cleft so far described, with the most pronounced remodeling. When the *Mt*-NDPK sequence was aligned with those of other hexameric NDPKs, including several mammalian isoforms (figure S5B), the $\alpha_A-\alpha_2$ hairpin was one of the least conserved regions of the protein, in agreement with the potentially important structural plasticity. On the basis of the R80A structure and the *Mt*-NDPK HDX-MS analysis, we propose that some NDPKs could interconvert between closed and open conformations, the latter being more accessible to bulky substrates (Figure 5). For a better understanding of the

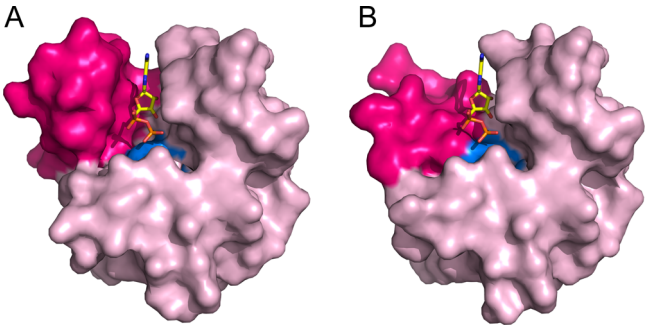

Figure 5. Surface view of the monomer in the (A) closed and (B) open conformations. α_A and α_2 helices are colored magenta, and the catalytic His117 is colored cyan. ADP is bound in the active site by homology with NDPK-A.[37]

histidine kinase activity of NDPKs, we plan to perform H/D continuous labeling experiments with different human isoforms: H1 and H2, which present this activity, and isoforms H3 and H4, which do not. Applying HDX-MS technology to study how SK4 channels are activated by isoform H2[7,16,56] will be part of our future research program for better understanding the mechanism of the histidine kinase activity of NDPKs.[55]

■ ASSOCIATED CONTENT

Supporting Information

The Supporting Information is available free of charge on the ACS Publications website at DOI: 10.1021/acs.biochem.8b01308.

Figures S1−S5 (PDF)

Accession Codes

NDK, UniProtKB entry A5U5E1; Protein Data Bank entry 6QA2.

■ AUTHOR INFORMATION

Corresponding Author

*Sorbonne Universités, UPMC Univ. Paris 06, CNRS, Laboratoire de Biologie Moléculaire et Cellulaire des Eucaryotes, UMR8226, Institut de Biologie Physico-Chimique, 13 rue Pierre et Marie Curie, 75005 Paris, France. E-mail: georgescauld@ibpc.fr.

ORCID

Alain Dautant: 0000-0002-7145-278X

Funding

This work was supported by the Foundation ARC pour la recherche sur le cancer and ITMO cancer-Plan Cancer 2014−2019 (France) (Grant SFI20101201793 to F.G. and P.M.). The French National Research Agency supported A.D. (ANR-

DOI: 10.1021/acs.biochem.8b01308
Biochemistry XXXX, XXX, XXX−XXX

12-BSV8-024) and P.M. (ANR-16-CE11-0032-03 and ANR-11-LABX-0011-01).

Notes

The authors declare no competing financial interest.

■ ACKNOWLEDGMENTS

The authors thank the European Synchrotron Radiation Facility (ESRF, Grenoble, France) and SOLEIL (Paris, France) for the provision of synchrotron radiation facilities and for assistance in using beamline PROXIMA. Pr. Anna Giartosio and Pr. Ioan Lascu are acknowledged for their encouragement and support in the realization of this research. Dr. Christophe Marchand and Miss Marion Hamon from the IBPC mass spectrometry platform are acknowledged for the performance of preliminary experiments.

■ REFERENCES

(1) Boissan, M., Schlattner, U., and Lacombe, M. L. (2018) The NDPK/NME superfamily: state of the art. *Lab. Invest. 98*, 164−174.

(2) Janin, J., and Deville-Bonne, D. (2002) Nucleoside-diphosphate kinase: structural and kinetic analysis of reaction pathway and phosphohistidine intermediate. *Methods Enzymol. 354*, 118−134.

(3) Lascu, I., and Gonin, P. (2000) The catalytic mechanism of nucleoside diphosphate kinases. *J. Bioenerg. Biomembr. 32*, 237−246.

(4) Janin, J., Dumas, C., Moréra, S., Xu, Y., Meyer, P., Chiadmi, M., and Cherfils, J. (2000) Three-dimensional structure of nucleoside diphosphate kinase. *J. Bioenerg. Biomembr. 32*, 215−225.

(5) Boissan, M., Montagnac, G., Shen, Q., Griparic, L., Guitton, J., Romao, M., Sauvonnet, N., Lagache, T., Lascu, I., Raposo, G., Desbourdes, C., Schlattner, U., Lacombe, M. L., Polo, S., van der Bliek, A. M., Roux, A., and Chavrier, P. (2014) Membrane trafficking. Nucleoside diphosphate kinases fuel dynamin superfamily proteins with GTP for membrane remodeling. *Science 344*, 1510−1515.

(6) Zala, D., Schlattner, U., Desvignes, T., Bobe, J., Roux, A., Chavrier, P., and Boissan, M. (2017) The advantage of channeling nucleotides for very processive functions. *F1000Research 6*, 724.

(7) Attwood, P. V., and Wieland, T. (2015) Nucleoside diphosphate kinase as protein histidine kinase. *Naunyn-Schmiedeberg's Arch. Pharmacol. 388*, 153−160.

(8) Puts, G. S., Leonard, M. K., Pamidimukkala, N. V., Snyder, D. E., and Kaetzel, D. M. (2018) Nuclear functions of NME proteins. *Lab. Invest. 98*, 211−218.

(9) Desvignes, T., Fauvel, C., and Bobe, J. (2011) The NME gene family in zebrafish oogenesis and early development. *Naunyn-Schmiedeberg's Arch. Pharmacol. 384*, 439−449.

(10) Marino, N., Nakayama, J., Collins, J. W., and Steeg, P. S. (2012) Insights into the biology and prevention of tumor metastasis provided by the Nm23 metastasis suppressor gene. *Cancer Metastasis Rev. 31*, 593−603.

(11) Khan, I., and Steeg, P. S. (2018) Metastasis suppressors: functional pathways. *Lab. Invest. 98*, 198−210.

(12) Steeg, P. S., Bevilacqua, G., Kopper, L., Thorgeirsson, U. P., Talmadge, J. E., Liotta, L. A., and Sobel, M. E. (1988) Evidence for a novel gene associated with low tumor metastatic potential. *J. Natl. Cancer Inst. 80*, 200−204.

(13) Khan, I., and Steeg, P. S. (2018) The relationship of NM23 (NME) metastasis suppressor histidine phosphorylation to its nucleoside diphosphate kinase, histidine protein kinase and motility suppression activities. *Oncotarget 9*, 10185−10202.

(14) Lu, Z., and Hunter, T. (2018) Metabolic Kinases Moonlighting as Protein Kinases. *Trends Biochem. Sci. 43*, 301−310.

(15) Adam, K., and Hunter, T. (2018) Histidine kinases and the missing phosphoproteome from prokaryotes to eukaryotes. *Lab. Invest. 98*, 233−247.

(16) Attwood, P. V. (2013) Histidine kinases from bacteria to humans. *Biochem. Soc. Trans. 41*, 1023−1028.

(17) Zhang, Q., McCorkle, J. R., Novak, M., Yang, M., and Kaetzel, D. M. (2011) Metastasis suppressor function of NM23-H1 requires its 3′-5′ exonuclease activity. *Int. J. Cancer 128*, 40−50.

(18) Jarrett, S. G., Novak, M., Dabernat, S., Daniel, J. Y., Mellon, I., Zhang, Q., Harris, N., Ciesielski, M. J., Fenstermaker, R. A., Kovacic, D., Slominski, A., and Kaetzel, D. M. (2012) Metastasis suppressor NM23-H1 promotes repair of UV-induced DNA damage and suppresses UV-induced melanomagenesis. *Cancer Res. 72*, 133−143.

(19) Lascu, I., Giartosio, A., Ransac, S., and Erent, M. (2000) Quaternary structure of nucleoside diphosphate kinases. *J. Bioenerg. Biomembr. 32*, 227−236.

(20) Georgescauld, F., Moynié, L., Habersetzer, J., Cervoni, L., Mocan, I., Borza, T., Harris, P., Dautant, A., and Lascu, I. (2013) Intersubunit ionic interactions stabilize the nucleoside diphosphate kinase of *Mycobacterium tuberculosis*. *PLoS One 8*, No. e57867.

(21) Moynié, L., Giraud, M. F., Georgescauld, F., Lascu, I., and Dautant, A. (2007) The structure of the *Escherichia coli* nucleoside diphosphate kinase reveals a new quaternary architecture for this enzyme family. *Proteins: Struct., Funct., Genet. 67*, 755−765.

(22) Potel, C. M., Fasci, D., and Heck, A. J. R. (2018) Mix and match of the tumor metastasis suppressor Nm23 protein isoforms *in vitro* and *in vivo*. *FEBS J. 285*, 2856−2868.

(23) Lascu, I., Chaffotte, A., Limbourg-Bouchon, B., and Veron, M. (1992) A Pro/Ser substitution in nucleoside diphosphate kinase of *Drosophila melanogaster* (mutation killer of prune) affects stability but not catalytic efficiency of the enzyme. *J. Biol. Chem. 267*, 12775−12781.

(24) Chen, Y., Moréra, S., Mocan, J., Lascu, I., and Janin, J. (2002) X-ray structure of *Mycobacterium tuberculosis* nucleoside diphosphate kinase. *Proteins: Struct., Funct., Genet. 47*, 556−557.

(25) Sun, J., Wang, X., Lau, A., Liao, T. Y., Bucci, C., and Hmama, Z. (2010) Mycobacterial nucleoside diphosphate kinase blocks phagosome maturation in murine RAW 264.7 macrophages. *PLoS One 5*, No. e8769.

(26) Ganaie, A. A., Lella, R. K., Solanki, R., and Sharma, C. (2011) Thermostable hexameric form of Eis (Rv2416c) protein of *M. tuberculosis* plays an important role for enhanced intracellular survival within macrophages. *PLoS One 6*, No. e27590.

(27) Sun, J., Singh, V., Lau, A., Stokes, R. W., Obregon-Henao, A., Orme, I. M., Wong, D., Av-Gay, Y., and Hmama, Z. (2013) *Mycobacterium tuberculosis* nucleoside diphosphate kinase inactivates small GTPases leading to evasion of innate immunity. *PLoS Pathog. 9*, No. e1003499.

(28) Dautant, A., Meyer, P., and Georgescauld, F. (2017) Hydrogen/Deuterium exchange mass spectrometry reveals mechanistic details of activation of nucleoside diphosphate kinases by oligomerization. *Biochemistry 56*, 2886−2896.

(29) Powell, H. R., Johnson, O., and Leslie, A. G. (2013) Autoindexing diffraction images with iMosflm. *Acta Crystallogr., Sect. D: Biol. Crystallogr. 69*, 1195−1203.

(30) Winn, M. D., Ballard, C. C., Cowtan, K. D., Dodson, E. J., Emsley, P., Evans, P. R., Keegan, R. M., Krissinel, E. B., Leslie, A. G., McCoy, A., McNicholas, S. J., Murshudov, G. N., Pannu, N. S., Potterton, E. A., Powell, H. R., Read, R. J., Vagin, A., and Wilson, K. S. (2011) Overview of the CCP4 suite and current developments. *Acta Crystallogr., Sect. D: Biol. Crystallogr. 67*, 235−242.

(31) Vagin, A., and Teplyakov, A. (2010) Molecular replacement with MOLREP. *Acta Crystallogr., Sect. D: Biol. Crystallogr. 66*, 22−25.

(32) Wales, T. E., Fadgen, K. E., Gerhardt, G. C., and Engen, J. R. (2008) High-speed and high-resolution UPLC separation at zero degrees Celsius. *Anal. Chem. 80*, 6815−6820.

(33) Wales, T. E., and Engen, J. R. (2006) Hydrogen exchange mass spectrometry for the analysis of protein dynamics. *Mass Spectrom. Rev. 25*, 158−170.

(34) Burkitt, W., and O'Connor, G. (2008) Assessment of the repeatability and reproducibility of hydrogen/deuterium exchange mass spectrometry measurements. *Rapid Commun. Mass Spectrom. 22*, 3893−3901.

DOI: 10.1021/acs.biochem.8b01308
Biochemistry XXXX, XXX, XXX−XXX

(35) Houde, D., Berkowitz, S. A., and Engen, J. R. (2011) The utility of hydrogen/deuterium exchange mass spectrometry in biopharmaceutical comparability studies. *J. Pharm. Sci. 100*, 2071−2086.
(36) Hu, Y.-S., Feng, F., and Liu, Y.-F. (2015) Structural and functional characterization of *Acinetobacter baumannii* nucleoside diphosphate kinase. *Shengwu Huaxue Yu Shengwu Wuli Jinzhan 42*, 260−267.
(37) Giraud, M. F., Georgescauld, F., Lascu, I., and Dautant, A. (2006) Crystal structures of S120G mutant and wild type of human nucleoside diphosphate kinase A in complex with ADP. *J. Bioenerg. Biomembr. 38*, 261−264.
(38) Souza, T. A., Trindade, D. M., Tonoli, C. C., Santos, C. R., Ward, R. J., Arni, R. K., Oliveira, A. H., and Murakami, M. T. (2011) Molecular adaptability of nucleoside diphosphate kinase b from trypanosomatid parasites: stability, oligomerization and structural determinants of nucleotide binding. *Mol. BioSyst. 7*, 2189−2195.
(39) Mishra, A. K., Singh, N., Agnihotri, P., Mishra, S., Singh, S. P., Kolli, B. K., Chang, K. P., Sahasrabuddhe, A. A., Siddiqi, M. I., and Pratap, J. V. (2017) Discovery of novel inhibitors for Leishmania nucleoside diphosphatase kinase (NDK) based on its structural and functional characterization. *J. Comput.-Aided Mol. Des. 31*, 547−562.
(40) Konermann, L., Vahidi, S., and Sowole, M. A. (2014) Mass spectrometry methods for studying structure and dynamics of biological macromolecules. *Anal. Chem. 86*, 213−232.
(41) Engen, J. R., and Wales, T. E. (2015) Analytical aspects of hydrogen exchange mass spectrometry. *Annu. Rev. Anal. Chem. 8*, 127−148.
(42) Marciano, D. P., Dharmarajan, V., and Griffin, P. R. (2014) HDX-MS guided drug discovery: small molecules and biopharmaceuticals. *Curr. Opin. Struct. Biol. 28*, 105−111.
(43) Engen, J. R., Wales, T. E., Chen, S., Marzluff, E. M., Hassell, K. M., Weis, D. D., and Smithgall, T. E. (2013) Partial cooperative unfolding in proteins as observed by hydrogen exchange mass spectrometry. *Int. Rev. Phys. Chem. 32*, 96−127.
(44) Panjarian, S., Iacob, R. E., Chen, S., Engen, J. R., and Smithgall, T. E. (2013) Structure and dynamic regulation of Abl kinases. *J. Biol. Chem. 288*, 5443−5450.
(45) Cervoni, L., Egistelli, L., Mocan, I., Giartosio, A., and Lascu, I. (2003) Quaternary structure of *Dictyostelium discoideum* nucleoside diphosphate kinase counteracts the tendency of monomers to form a molten globule. *Biochemistry 42*, 14599−14605.
(46) Boissier, F., Georgescauld, F., Moynié, L., Dupuy, J. W., Sarger, C., Podar, M., Lascu, I., Giraud, M. F., and Dautant, A. (2012) An intersubunit disulfide bridge stabilizes the tetrameric nucleoside diphosphate kinase of *Aquifex aeolicus*. *Proteins: Struct., Funct., Genet. 80*, 1658−1668.
(47) Pedelacq, J. D., Waldo, G. S., Cabantous, S., Liong, E. C., and Terwilliger, T. C. (2005) Structural and functional features of an NDP kinase from the hyperthermophile crenarchaeon *Pyrobaculum aerophilum*. *Protein Sci. 14*, 2562−2573.
(48) Yonezawa, Y., Izutsu, K., Tokunaga, H., Maeda, H., Arakawa, T., and Tokunaga, M. (2007) Dimeric structure of nucleoside diphosphate kinase from moderately halophilic bacterium: Contrast to the tetrameric pseudomonas counterpart. *FEMS Microbiol. Lett. 268*, 52−58.
(49) Arai, S., Yonezawa, Y., Okazaki, N., Matsumoto, F., Tamada, T., Tokunaga, H., Ishibashi, M., Blaber, M., Tokunaga, M., and Kuroki, R. (2012) A structural mechanism for dimeric to tetrameric oligomer conversion in *halomonas* sp. nucleoside diphosphate kinase. *Protein Sci. 21*, 498−510.
(50) DeLano, W. L. (2002) *The PyMOL Molecular Graphics System*, DeLano Scientific, Palo Alto, CA.
(51) Georgescauld, F., Moynié, L., Habersetzer, J., and Dautant, A. (2014) Structure of *Mycobacterium tuberculosis* nucleoside diphosphate kinase R80N mutant in complex with citrate. *Acta Crystallogr., Sect. F: Struct. Biol. Commun. 70*, 40−43.
(52) Dexheimer, T. S., Carey, S. S., Zuohe, S., Gokhale, V. M., Hu, X., Murata, L. B., Maes, E. M., Weichsel, A., Sun, D., Meuillet, E. J., Montfort, W. R., and Hurley, L. H. (2009) NM23-H2 may play an indirect role in transcriptional activation of c-myc gene expression but does not cleave the nuclease hypersensitive element III1. *Mol. Cancer Ther. 8*, 1363−1377.
(53) Kumar, P., Verma, A., Saini, A. K., Chopra, P., Chakraborti, P. K., Singh, Y., and Chowdhury, S. (2005) Nucleoside diphosphate kinase from *Mycobacterium tuberculosis* cleaves single strand DNA within the human c-myc promoter in an enzyme-catalyzed reaction. *Nucleic Acids Res. 33*, 2707−2714.
(54) Saini, A. K., Maithal, K., Chand, P., Chowdhury, S., Vohra, R., Goyal, A., Dubey, G. P., Chopra, P., Chandra, R., Tyagi, A. K., Singh, Y., and Tandon, V. (2004) Nuclear localization and in situ DNA damage by *Mycobacterium tuberculosis* nucleoside-diphosphate kinase. *J. Biol. Chem. 279*, 50142−50149.
(55) Webb, P. A., Perisic, O., Mendola, C. E., Backer, J. M., and Williams, R. L. (1995) The crystal structure of a human nucleoside diphosphate kinase, NM23-H2. *J. Mol. Biol. 251*, 574−587.
(56) Zhou, X. B., Feng, Y. X., Sun, Q., Lukowski, R., Qiu, Y., Spiger, K., Li, Z., Ruth, P., Korth, M., Skolnik, E. Y., Borggrefe, M., Dobrev, D., and Wieland, T. (2015) Nucleoside diphosphate kinase B-activated intermediate conductance potassium channels are critical for neointima formation in mouse carotid arteries. *Arterioscler., Thromb., Vasc. Biol. 35* (8), 1852−1861.

DOI: 10.1021/acs.biochem.8b01308
Biochemistry XXXX, XXX, XXX−XXX